20. PALEOMAGNETISM OF THE IGNEOUS SECTION, HOLE 1213B, SHATSKY RISE[1]

M. Tominaga,[2] W.W. Sager,[2] and J.E.T. Channell[3]

ABSTRACT

Paleomagnetic measurements were made on 52 samples from the igneous section of Ocean Drilling Program Hole 1213B for the purpose of determining paleoinclination and polarity and giving insight about volcanic emplacement. Samples were taken at approximately even intervals from the three basaltic sills that make up the section, and all samples were demagnetized using an alternating field or thermal methods in an effort to determine the characteristic magnetization direction. Half of the samples gave inconsistent results. Furthermore, natural remanent magnetization values were strong and median destructive field values were low, implying that the basalts are prone to acquiring an overprint from the drill string. In addition, hysteresis results show low coercivities and lie in the pseudosingle-domain field of a Day plot (M_r/M_s vs. B_{cr}/B_c). All of these observations suggest that the samples are characterized by a low-coercivity magnetic mineral, such as titanomagnetite, that may not always preserve a stable characteristic remanence. Nevertheless, 26 samples produced consistent inclinations, giving shallow, negative values that are considered the likely characteristic direction. There is no statistical difference between mean inclinations for the three units, implying they erupted within a short time. Measurements from all reliable samples were averaged to give a paleoinclination of –9.3° with 95% confidence limits from –41.8° to 27.5°, the large uncertainty resulting from the fact that paleosecular variation is not averaged. Although the large uncertainty makes a unique assignment of polarity difficult, the interpretation that is most consistent with other Pacific paleomagnetic data is that the magnetization has a reversed polarity acquired slightly north of the equator.

INTRODUCTION

During Ocean Drilling Program (ODP) Leg 198, 46 m of basalt was cored at Site 1213 (31°34.6402′N, 157°17.8605′E) on the flank of the Southern High of Shatsky Rise (Fig. F1). The basement section consists of three basaltic sills of approximately equal thickness (Table T1), intruded into Berriasian age (lowest Cretaceous) pelagic sediments (Shipboard Scientific Party, 2002). These three igneous units were interpreted as sills because they are thick (>7 m), massive igneous units, they have a coarse-grained texture that becomes finer toward chilled margins at top and bottom, vesicles and contraction cracks occur preferentially at the margins, and metamorphosed sediments are found above and intercalated with the igneous units (Shipboard Scientific Party, 2002). Two samples from the sills have been dated using $^{40}Ar/^{39}Ar$ radiometric techniques, producing indistinguishable dates that average 144.6 ± 0.8 Ma (2σ error) (Mahoney et al., 2005; Sager, in press b).

Paleomagnetic data from basaltic cores are important because they give a reading of paleolatitude of the plate at the age of rock formation. Results from a small number of units, as were cored at Site 1213, have limited use by themselves because they do not properly average paleosecular variation. Nevertheless, they are important because they can be combined with other paleomagnetic data of similar age (Peirce, 1976; Cox and Gordon, 1984). In addition, few data of Jurassic or Early Cretaceous age are available for the Pacific plate (Larson et al., 1992). Our motivation in this study was to determine paleoinclinations of Site 1213 basalt units to give geologic insights about the basement of Shatsky Rise (e.g., how fast the basement erupted, polarity, and a hint at paleolatitude). Paleomagnetic data from the Berriasian host sediments are given in a companion article (Sager et al., this volume).

METHOD

A total of 52 samples from Hole 1213B were measured in this study (Table T1). Samples were obtained as 2.5-cm-diameter minicores drilled perpendicular to the split face of the rock cores. Only larger core pieces, believed to be vertically oriented, were sampled. These samples were spaced at irregular intervals in rock sections, with the objective of collecting about the same number from each sill.

Sample magnetizations were measured with a Geofyzika JR-5A spinner magnetometer. Both alternating-field (AF) and thermal demagnetization were carried out on different suites of samples to remove overprint magnetizations and to isolate the characteristic remanent magnetization. For the AF method, samples were demagnetized with a Schoenstedt Instruments AC demagnetizer model GSD-1 and for thermal treatments, samples were demagnetized with a Schoenstedt Instruments model TSD-1. All measurements were made within shielded rooms at the University of Houston, Texas (USA), paleomagnetic laboratory.

Approximately 60% of samples were treated with the AF method, usually with 2.5- to 5.0-mT steps up to 30–40 mT. Higher steps were not often used because most samples gave inconsistent directions when treated with higher fields. The rest of the samples were treated with thermal demagnetization, typically with 50°C steps in the range of 150° to 600°C, except for 12 samples that were examined in detail from 500°

F1. Site 1213 location, p. 8.
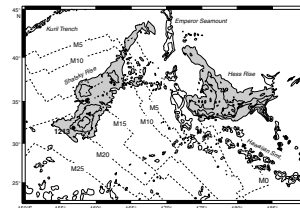
T1. Paleomagnetic measurements from Hole 1213B basalt samples, p. 14.

to 580°C with 20°C steps to look at directions above 500°C. See the "Supplementary Material" contents list for AF and thermal demagnetization data tables.

Hysteresis loops for 10 representative samples were measured using a Princeton Instruments Micromag model 2900 alternating-gradient magnetometer at the University of California, Davis (USA), paleomagnetic laboratory. Volume susceptibility was measured at Texas A&M University, College Station, Texas (USA), with a Bartington MS-2 susceptibility meter.

Characteristic magnetization directions were calculated using principal component analysis (PCA) (Kirschvink, 1980). We chose two to six (average of four) steps that appeared to have univectorial decay toward the orthogonal vector diagram origin. Sample directions were calculated using PCA with the solution not anchored to the origin when that method gave a solution apparently consistent with the observed demagnetization trends in orthogonal vector plots. If it did not, we used a PCA constrained to pass through the origin.

Individual sample magnetizations were averaged using the method of Cox and Gordon (1984). Following this method, paleoinclinations were treated as colatitudes and averaged for each lithologic unit and unit means were tested for statistical distinctness. The mean paleocolatitude was calculated and corrected for bias inherent in azimuthally unoriented data, and 95% confidence limits were estimated. In the calculation of confidence limits, the Cox and Gordon (1984) method includes an estimate of error caused by secular variation as well as off-vertical tilt of the borehole (assumed 2° or less).

RESULTS

Natural remanent magnetization (NRM) measurements have a range of 1.4 to 32.9 A/m (median value = 7.5 A/m) (Table T1). These NRM values are in the range of values reported for ocean crustal basalts (Johnson et al., 1996), although they are on the strong side of average. On orthogonal vector diagrams, the NRM is often a steep, downward-pointing vector. This is commonly observed with ODP samples and is attributed to overprint by the drill string (Acton et al., 2002).

AF demagnetizations give low median destructive field (MDF) values in the range of 2.5 to 5.9 mT (Fig. F2; Table T1). Most samples had only negligible magnetization remaining after the 30-mT demagnetization step. This suggests that the magnetization has a low coercivity and is susceptible to acquiring an overprint. Because the magnetization weakens rapidly with demagnetization, we attribute much of the strong NRM values to this overprint. AF and thermal demagnetization results showed three types of behavior. A total of 18 samples (29%) gave scattered directions, making the calculation of a characteristic remanence direction inappropriate. Samples with poor demagnetization results were often physically close to one another in the cores, suggesting lithology as a factor. For example, the upper part of Unit 3 has a large number of inconsistent samples (Table T1). Of the samples that produced consistent demagnetization results, 7 gave positive inclinations (e.g., Samples 198-1213B-31R-6, 69–72 cm, and 31R-1, 45–47 cm) (Fig. F2) and 27 gave shallow, negative inclinations (e.g., Samples 31R-2, 36–38 cm, and 32R-5, 54–56 cm) (Fig. F2). We think that the negative inclinations, being more prevalent and consistent, likely represent the true characteristic remanence (see "Discussion and Conclusions," p. 4).
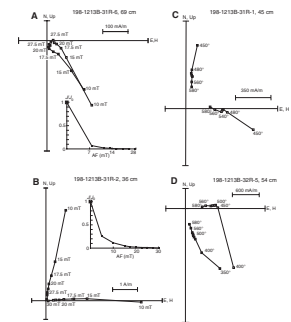
The positive inclinations may come from samples from which the drill string overprint was incompletely removed.

Hysteresis measurements range from 3.6 to 13.6 mT in saturation coercivity (Fig. F3), and for remanence coercivity, low values are consistent with the MDF results (Table T1). Low coercivity and hysteresis curves that rapidly reach saturation may indicate that titanomagnetite is the predominant type of magnetic grain. On a Day plot (M_r/M_s vs. B_{cr}/B_c), Hole 1213B samples plot to the left of published curves for single-domain and multidomain grain mixtures (Fig. F4). The displacement from model curves is probably a result of the samples having grains with different shape and composition characteristics compared to those assumed for the simple mixing model. However, the trend of Hole 1213B samples is more or less parallel with the mixing curves, implying that a similar phenomenon occurs in these samples. The vertical position of Hole 1213B samples on this diagram suggests that the magnetic behavior results from a mixture of single-domain and multidomain grains with a large fraction of the latter. Multidomain grains often have magnetizations that are easily modified by applied magnetic fields, and this factor may be responsible for the inconsistent demagnetization behavior of many samples.

DISCUSSION AND CONCLUSIONS

It was our objective to determine the paleoinclination of the Site 1213 sills. We found many samples with a consistent shallow negative inclination in the range –0.8° to –26°, but usually between –5° and –15°. These inclinations are interpreted as the initial, characteristic remanence magnetization recorded in the sills. We do not think the positive-inclination samples are representative of the true magnetization direction for several reasons. Most samples are overprinted by a steep, downward-pointing magnetization imparted by the drill string (e.g., Acton et al., 2002). In most of the positive-inclination samples, the overprint and final characteristic magnetization direction appear to overlap, with a gradual shift from the former to the latter during progressive demagnetization. This observation suggests that the overprint may not be completely removed. Furthermore, the positive inclinations show more scatter than the negative (Fig. F5), which is consistent with variable removal of the drill string overprint. In addition, the positive inclinations are mixed with negative inclinations in Unit 2 (Fig. F5). This observation implies that positive-inclination values do not represent a separate unit with a different magnetization direction but are instead a spurious direction. In Unit 1, the positive inclinations are grouped, and we could interpret them as a separate unit, but the simplest explanation is that these inclinations are samples in which the downward, positive drill string overprint has not been completely removed.

Mean inclinations in the three sills are not statistically distinct. The similarity in the paleoinclination of the three units probably means that the units erupted during a short time interval. Averaging all 26 samples with reliable negative inclination values gives a mean inclination of –9.3°. Although the tight clustering of inclination values results in a standard deviation of only 4.3°, the low scatter is not indicative of the true accuracy of the paleoinclination because inclination variation caused by secular variation has not been averaged out. The Cox and Gordon (1984) method uses a model of secular variation to propagate the uncertainty owing to secular variation into uncertainty estimates.
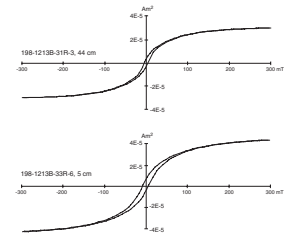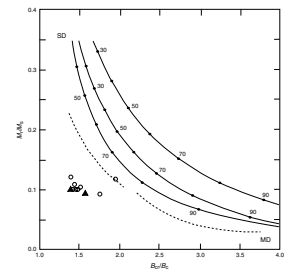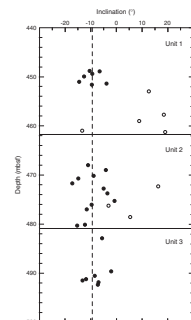
The model standard error for secular variation at Hole 1213 is 9.1° in colatitude (Cox and Gordon, 1984). When combined with an estimate of 2° for the uncertainty in the vertical orientation of the borehole and the observed scatter in inclination values (Cox and Gordon, 1984), this method gives 95% confidence limits spanning 69° for paleoinclination (–41.8° to 27.5°) and 38.6° for paleolatitude (–24.0° to 14.6°). This large uncertainty stems from the fact that all of the measurements amount to a single spot reading of the geomagnetic field and thus paleosecular variation is poorly averaged.

Demagnetization and hysteresis experiments suggest that the Hole 1213B basalts contain low-coercivity magnetite grains that easily acquire an overprint, probably from the drill string, resulting in high NRM values. Interestingly, our results are similar to those from sills cored at Deep Sea Drilling Project (DSDP) Site 462 (Steiner, 1981). This suggests that something about sills, perhaps a long cooling history that results in larger magnetic grain sizes, may cause unreliable magnetite behavior.

Because of the small number of units and low latitude, we cannot be certain of the polarity and true inclination. With a negative mean inclination, the polarity is reversed if the lithosphere was formed north of equator or normal if it was formed south of the equator. The explanation most consistent with other observations is a reversed polarity, formed north of the equator. Reversed polarity is consistent with the magnetic model of the Southern High, which gave a negative magnetization (Sager and Han, 1993). Furthermore, assuming reversed polarity, the colatitude arc is in better agreement with Late Jurassic and Early Cretaceous paleomagnetic poles determined from anomaly skewness (Larson and Sager, 1992), Jurassic and Early Cretaceous sediment data from the western Pacific (Steiner and Wallick, 1992), and other Pacific basalt core data (Fig. F6). Although the large uncertainty for Hole 1213B basalts does not allow us to rule out a normal polarity, the reversed polarity is a more consistent with other data.

ACKNOWLEDGMENTS
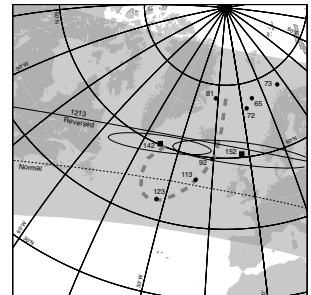
REFERENCES

Acton, G.D., and Gordon, R.G., 1991. A 65 Ma paleomagnetic pole for the Pacific plate from the skewness of magnetic Anomalies 27r-31. *Geophys. J. Int.,* 106:407–420.

Acton, G.D., Okada, M., Clement, B.M., Lund, S.P., and Williams, T., 2002. Paleomagnetic overprints in ocean sediment cores and their relationship to shear deformation caused by piston coring. *J. Geophys. Res.,* 107:10.1029/2001JB000518.

Cox, A., and Gordon, R.G., 1984. Paleolatitudes determined from paleomagnetic data from vertical cores. *Rev. Geophys. Space Phys.,* 22:47–72.

Dunlop, D.J., 2002a. Theory and application of the Day plot (M_{rs}/M_s versus H_{cr}/H_c), 1. Theoretical curves and tests using titanomagnetite data. *J. Geophys. Res.,* 107:10.1029/2001JB000486.

Dunlop, D.J., 2002b. Theory and application of the Day plot (M_{rs}/M_s versus H_{cr}/H_c), 2. Application to data for rocks, sediments, and soils. *J. Geophys. Res.,* 107:10.1029/2001JB000487.

Dunlop, D.J., and Prévot, M., 1982. Magnetic properties and opaque mineralogy of drilled submarine intrusive rocks. *Geophys. J. R. Astron. Soc.,* 69:763–802.

Johnson, H.P., Patten, D.V., and Sager, W.W., 1996. Age-dependent variation in the magnetization of seamounts. *J. Geophys. Res.,* 101:13701–13714.

Kirschvink, J.L., 1980. The least-squares line and plane and the analysis of palaeomagnetic data. *Geophys. J. R. Astron. Soc.,* 62:699–718.

Larson, R.L., and Sager, W.W., 1992. Skewness of magnetic Anomalies M0 to M29 in the northwestern Pacific. *In* Larson, R.L., Lancelot, Y., et al., *Proc. ODP, Sci. Results,* 129: College Station, TX (Ocean Drilling Program), 471–481.

Larson, R.L., Steiner, M.B., Erba, E., and Lancelot, Y., 1992. Paleolatitudes and tectonic reconstructions of the oldest portion of the Pacific plate: a comparative study. *In* Larson, R.L., Lancelot, Y., et al., *Proc. ODP, Sci. Results,* 129: College Station, TX (Ocean Drilling Program), 615–631.

Mahoney, J.J., Duncan, R.A., Tejada, M.L.G., and Sager, W.W., 2005. Geochemistry and age of basalts from Shatsky Rise, NW Pacific. *Geochim. Cosmochim. Acta,* 68 (suppl. 1):591. (abstract)

Peirce, J.W., 1976. Assessing the reliability of DSDP paleolatitudes. *J. Geophys. Res.,* 81:4173–4187.

Petronotis, K.E., and Gordon, R.G., 1999. A Maastrichtian palaeomagnetic pole for the Pacific plate from a skewness analysis of marine magnetic Anomaly 32. *Geophys. J. Int.,* 139:227–247.

Sager, W.W., 2003. A Chron 33r paleomagnetic pole for the Pacific plate. *Geophys. Res. Lett.,* 30:10.1029/2003GL017964.

Sager, W.W., in press a. Cretaceous basalt core paleomagnetic poles for the Pacific plate: implications for apparent polar wander and plate tectonics, *Phys. Earth Planet. Inter.*

Sager, W.W., in press b. What built Shatsky Rise, a mantle plume or ridge processes? *In* Foulger, G.R., Anderson, D.L., Natland, J.H., and Presnall, D.C. (Eds.), *Plumes, Plates, and Paradigms.* Spec. Pap.—Geol. Soc. Am.

Sager, W.W., and Han, H.-C., 1993. Rapid formation of the Shatsky Rise oceanic plateau inferred from its magnetic anomaly. *Nature,* 364:610–613.

Sager, W.W., and Pringle, M.S.,1988. Mid-Cretaceous to early Tertiary apparent polar wander path of the Pacific plate. *J. Geophys. Res.,* 93(11):753–771.

Shipboard Scientific Party, 2002. Site 1213. *In* Bralower, T.J., Premoli Silva, I., Malone, M.J., et al., *Proc. ODP, Init. Repts.,* 198, 1–110 [CD-ROM]. Available from: Ocean Drilling Program, Texas A&M University, College Station TX 77845-9547, USA.

Steiner, M.B., 1981. Paleomagnetism of the igneous complex, Site 462. *In* Larson, R.L., Schlanger, S.O., et al., *Init. Repts. DSDP,* 61: Washington (U.S. Govt. Printing Office), 717–729.

Steiner, M.B., and Wallick, B.P., 1992. Jurassic to Paleocene paleolatitudes of the Pacific plate derived from the paleomagnetism of the sedimentary sequences at Sites 800, 801, and 802. *In* Larson, R.L., Lancelot, Y., et al., *Proc. ODP, Sci. Results,* 129: College Station, TX (Ocean Drilling Program), 431–446.

Figure F1. Map showing location of Site 1213 and prominent bathymetric features of the northwest Pacific Ocean. Smt. = seamount.
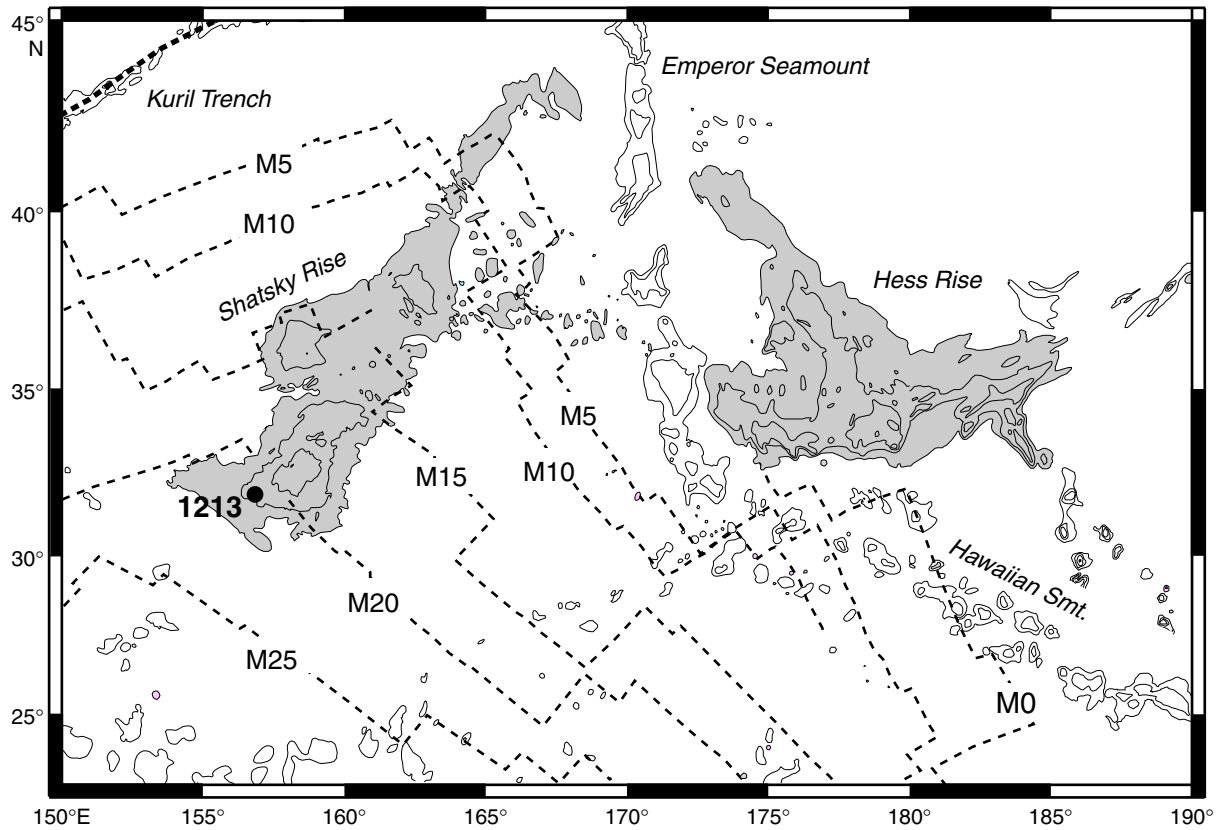
Figure F2. Example demagnetization results from Hole 1213B basalt samples. Plots show projection of magnetization vector endpoints on two orthogonal planes: horizontal (solid squares) and vertical (open squares). Numbers give strength of demagnetizing field (in milliTesla) or temperature of sample heating (in degrees centigrade). **A.** Alternating-field (AF) demagnetized sample from which the downward directed overprint is never completely removed. **B.** AF demagnetized sample that gives a shallow, negative characteristic magnetization. **C.** Thermally demagnetized sample for which heating did not completely remove the downward overprint. **D.** Thermally demagnetized sample which gives a shallow, negative inclination above 450°C. Inset plots show normalized magnetization and demonstrate large initial loss of magnetization at low AF demagnetization steps.
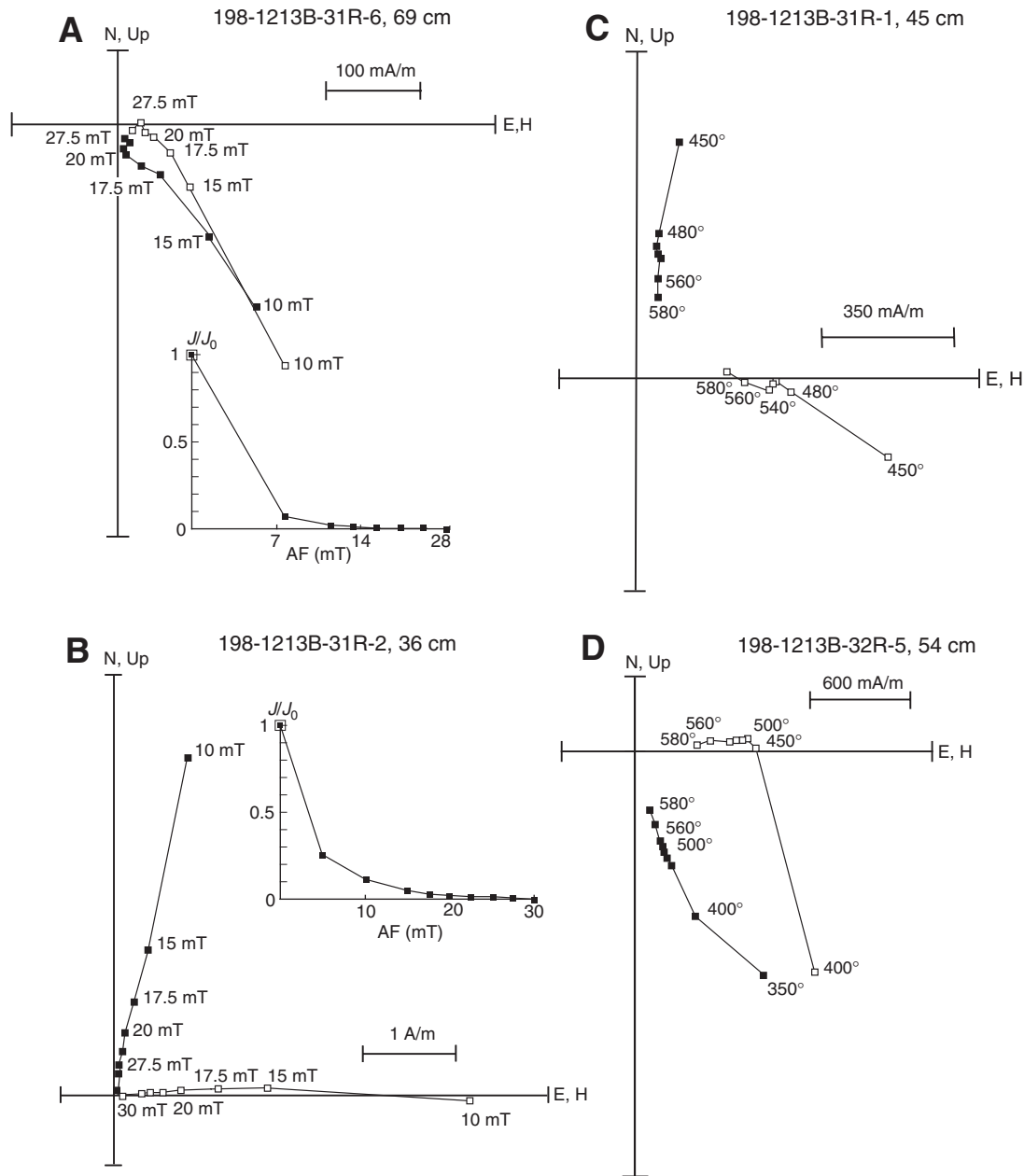
Figure F3. Hysteresis curves for two representative Hole 1213B basalt samples.
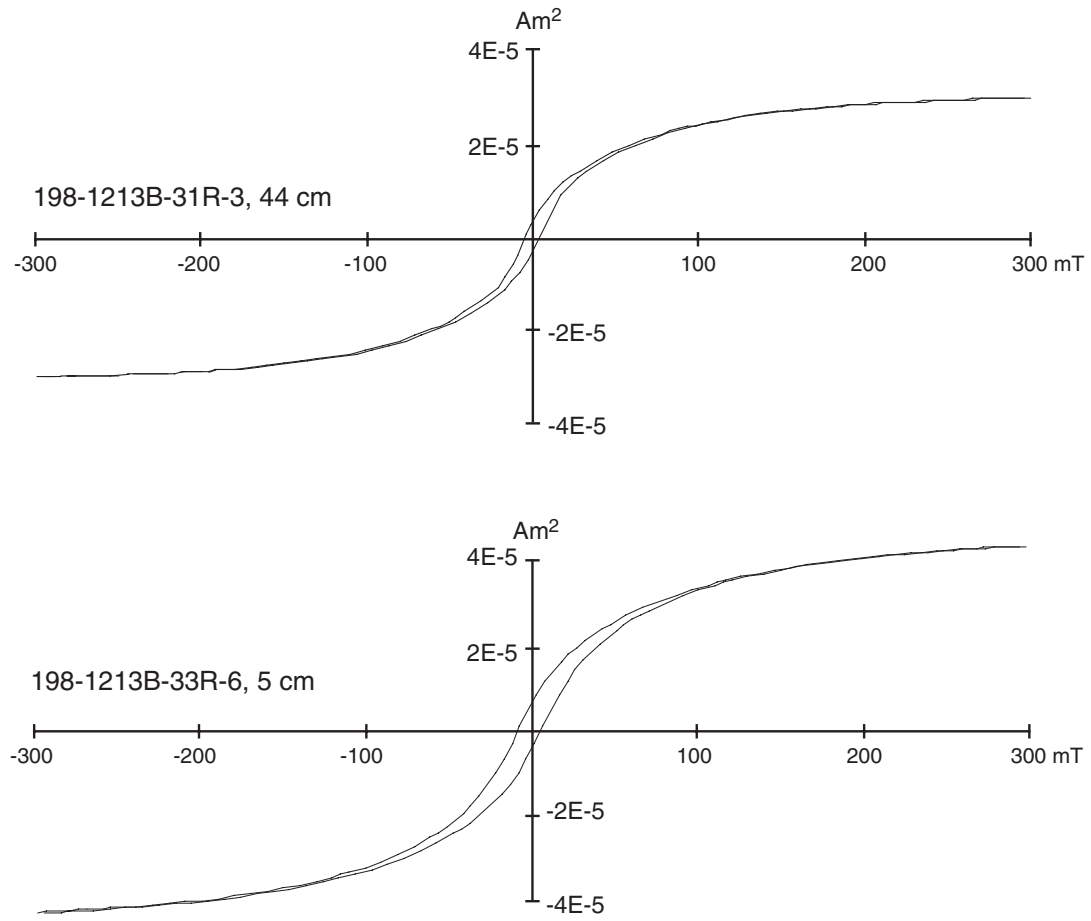
Figure F4. Plot of M_r/M_s (saturation remanence/saturation magnetization) vs. B_{cr}/B_c (remanent coercivity/ coercivity field) for Hole 1213B basalt samples. Open symbols denote samples that gave inconsistent demagnetization results, whereas solid triangles show samples that gave consistent results. Curves represent theoretical mixing model for single-domain (SD) and multidomain (MD) magnetite grains (Dunlop, 2002a, 2002b). Numbers at points along line give percentage of MD grains in mixture. Dashed lines show trends from some published dolerite, gabbro, and peridotite samples (Dunlop and Prévot, 1982).
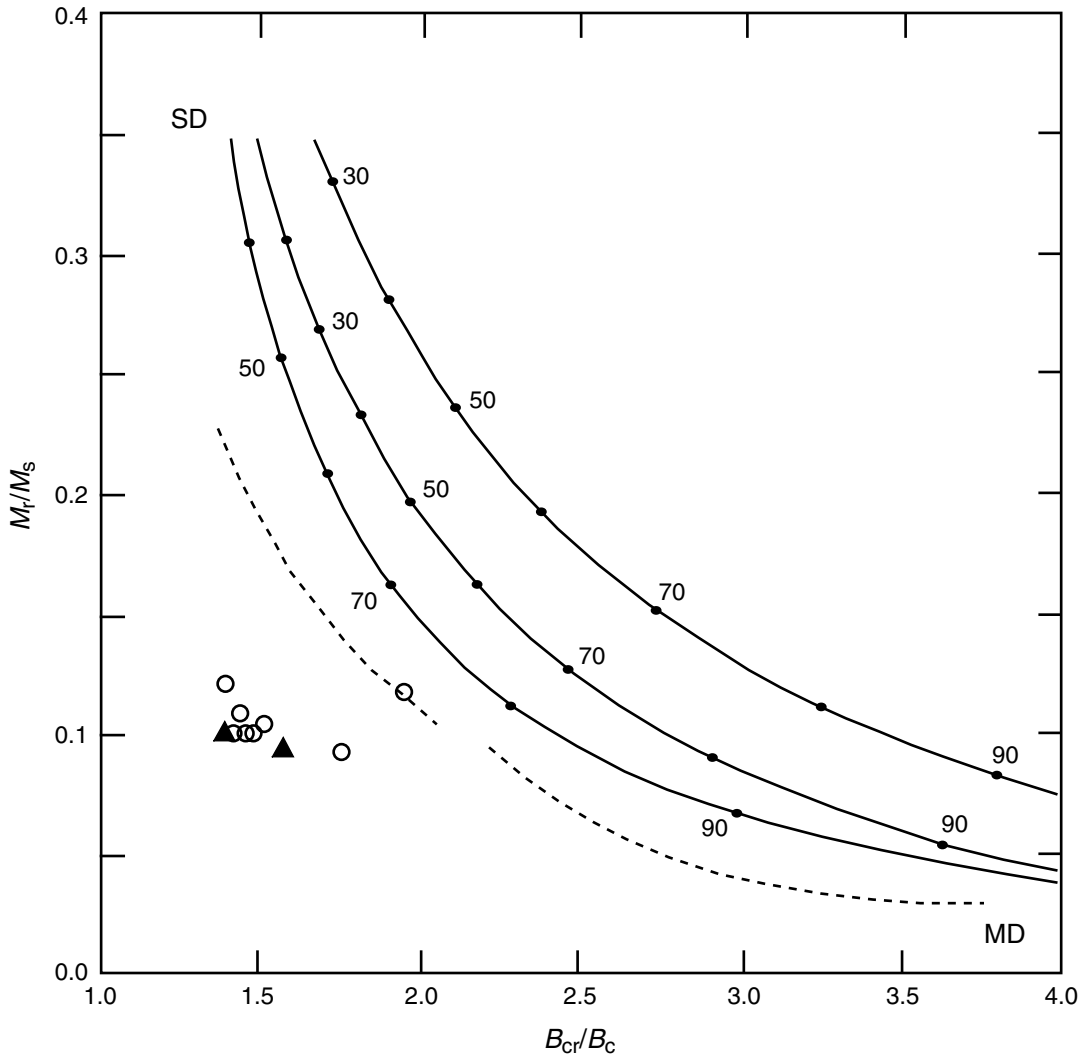
Figure F5. Characteristic magnetization inclinations for Hole 1213B basalt samples. Solid symbols denote those used to calculate the mean inclination (dashed line). Open symbols show inclinations not used for those calculations (see Table T1, p. 14). Horizontal lines show boundaries between three igneous units (sills).
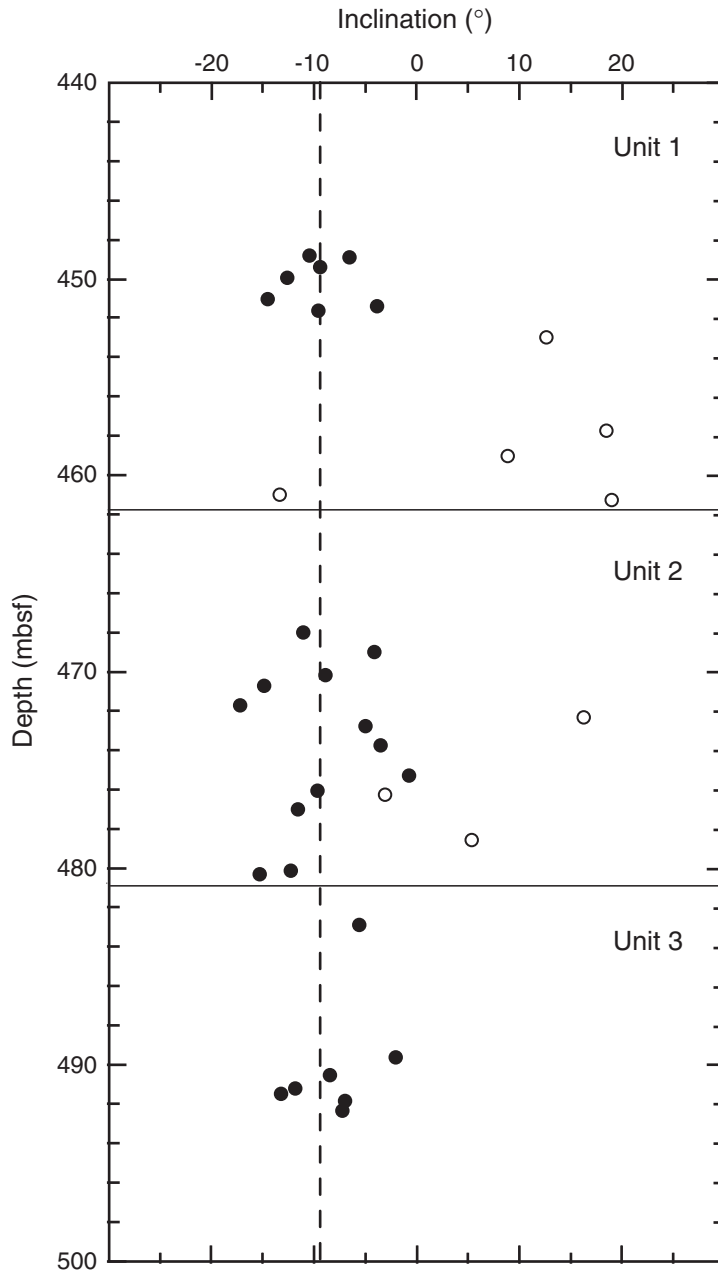
Figure F6. Colatitude arcs for Hole 1213B basalt samples compared with Cretaceous and Jurassic paleomagnetic poles. Solid squares show Jurassic (152 Ma) and Early Cretaceous (142 Ma) poles from magnetic lineation skewness (Larson and Sager, 1992). Solid circles are Late and mid-Cretaceous poles from other sources (72 Ma, Sager and Pringle, 1988; 65 Ma, Acton and Gordon, 1991; 73 Ma, Petronotis and Gordon, 1999; 81 Ma, Sager, 2003; 92, 113, and 123 Ma, Sager, in press a). Solid arc shows locus of poles predicted by assuming reversed polarity, whereas dashed arc shows locus of poles assuming normal polarity. Ellipses show 95% confidence regions for the Jurassic and Early Cretaceous poles; other pole error ellipses are omitted for clarity. Gray band shows estimated region of 95% confidence for the normal colatitude arc. Heavy dashed line shows trend of Pacific apparent polar wander path.
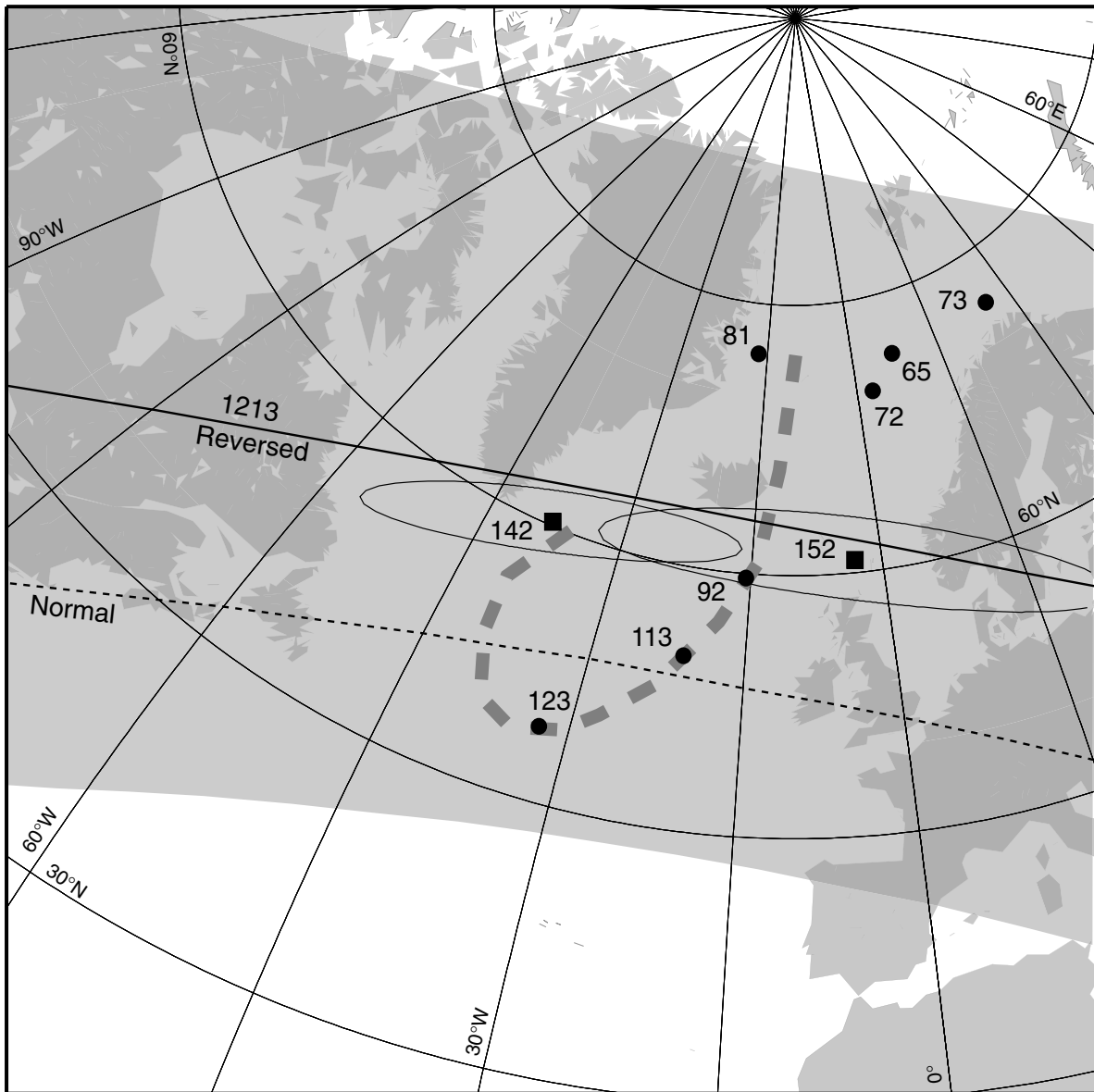
Table T1. Paleomagnetic measurements from Hole 1213B basalt samples. (**See table notes.** Continued on next page.)

Core, section, interval (cm)	Depth (mbsf)	NRM (A/m)	Incl. (°)	PCA type	MAD (°)	Demag type	Steps	N	MDF (mT)	B_c (mT)	B_{cr} (mT)	M_s (10^{-6} Am²)	M_r (10^{-6} Am²)	Susceptibility (10^{-5} SI)	Rejection criteria
Unit 1															
198-1213B-															
28R-1, 62	448.42	7.2				TH								0.030	NS
28R-1, 95	448.75	12.8	–10.6	A	1.00	TH	560–580	2						0.047	
28R-1, 107	448.87	9.0	–6.6	F	16.20	AF	20–30	5	3.46	4.60	6.36	28.81	3.49	0.033	
28R-2, 33	449.38	10.2	–9.7	A	0.80	TH	550–575	2						0.047	
28R-2, 83	449.88	21.9	–12.5	A	3.20	TH	540–580	3						0.036	
28R-2, 118	450.23	13.3				AF								0.029	NS
28R-3, 46	451.00	16.6	–14.4	F	10.70	AF	20–28	3	5.22	4.36	6.57	28.96	3.01	0.036	
28R-3, 79	451.33	16.0	–4.0	F	11.20	TH	480–580	5						0.050	
28R-3, 102	451.56	10.6	–9.7	F	7.50	TH	500–575	3						0.040	
29R-1, 21	453.01	3.0	12.7	F	11.40	AF	15–23	4	5.75	4.13	6.47	32.18	3.02	0.028	OV
29R-1, 58	453.38	7.7				AF								0.035	NS
30R-1, 39	457.79	9.1	18.3	F	4.80	AF	10–23	5	2.99					0.033	OV
30R-2, 46	459.10	12.4	8.9	F	14.10	AF	18–28	4	5.28	4.06	5.60	27.71	2.83	0.032	OV
30R-2, 95	459.59	6.0				TH								0.041	NS
30R-3, 44	460.53	1.8				AF								0.033	NS
30R-3, 116	461.25	1.4	–13.5*	F	26.30	AF	15–35	3	2.50					0.028	MA
30R-4, 16	461.71	5.1	19.0	F	12.10	TH	350–500	3						0.041	OV
Unit 2															
198-1213B-															
31R-1, 45	467.45	9.2				TH								0.028	NS
31R-1, 97	467.97	9.5	–11.2	F	9.20	TH	540–580	3						0.030	
31R-2, 36	468.70	32.9	–4.1	F	2.20	AF	22–28	4	3.36					0.032	
31R-2, 100	469.34	11.9	–9.9*	A	7.70	TH	550–575	2						0.023	OV
31R-3, 44	470.15	13.9	–8.8	F	1.00	AF	18–25	4	5.68	4.35	6.41	31.26	3.13	0.032	
31R-3, 100	470.71	11.4	–14.8	F	16.70	AF	20–28	4	5.36					0.030	
31R-4, 49	471.68	9.1	–17.3	F	3.30	AF	20–35	4	7.15					0.026	
31R-4, 108	472.27	7.1	16.8	F	2.10	AF	15–20	3	5.40					0.031	OV
31R-5, 16	472.77	6.5	–4.9	A	2.60	TH	450–500	2						0.032	
31R-5, 113	473.74	10.2	–3.5	F	8.40	AF	20–28	4	5.52					0.032	
31R-6, 69	474.68	4.9	49.9	F	14.20	AF	18–25	4	5.40					0.034	OV
31R-6, 134	475.33	6.8	–0.8	A	3.90	TH	450–575	4						0.035	
31R-7, 62	476.05	15.3	–9.8	F	9.90	AF	18–28	5	5.69	3.58	6.27	23.04	2.12	0.031	
31R-7, 88	476.31	7.1	–3.1	F	25.80	TH	480–560	5						0.026	MA
31R-8, 28	476.95	6.5	–11.5	F	19.10	AF	25–33	4	5.40					0.028	
32R-1, 40	477.00	10.9	–26.0*	F	22.20	AF	25–30	3	3.14					0.029	MA
32R-1, 91	477.51	11.5				AF								0.035	NS
32R-2, 40	478.50	6.2	5.2	F	1.80	TH	450–550	3						0.042	OV
32R-2, 85	478.95	4.9				AF								0.029	NS
32R-3, 60	480.14	2.4	–12.3	F	13.90	TH	450–520	4						0.061	
32R-3, 78	480.32	3.4	–15.3	A	8.30	TH	550–575	2						0.023	
32R-4, 39	481.28	4.0				TH								0.058	NS
Unit 3															
198-1213B-															
32R-4, 138	482.30	4.5				AF								0.026	NS
32R-5, 54	482.89	4.0	–5.7	F	4.80	TH	480–580	6						0.056	
33R-1, 104	486.70	6.8				AF				3.82	5.44	27.99	2.81	0.024	NS

Table T1 (continued).

Core, section, interval (cm)	Depth (mbsf)	NRM (A/m)	Incl. (°)	PCA type	MAD (°)	Demag type	Steps	N	MDF (mT)	B_c (mT)	B_{cr} (mT)	M_s (10^{-6} Am^2)	M_r (10^{-6} Am^2)	Susceptibility (10^{-5} SI)	Rejection criteria
33R-2, 4	487.24	9.1				AF				3.86	5.57	34.02	3.43	0.015	NS
33R-2, 60	487.80	10.2				TH								0.040	NS
33R-3, 34	488.40	8.0				AF								0.028	NS
33R-3, 88	488.94	8.0				AF								0.033	NS
33R-4, 32	489.69	3.8	−2.1	F	6.50	AF	15–30	4	3.36	4.19	6.02	33.27	3.61	0.024	
33R-5, 5	490.48	4.1	−8.5	F	19.90	TH	480–580	6						0.052	
33R-5, 63	491.06	6.0	−11.8	F	11.60	AF	22–28	4	5.37					0.031	
33R-5, 96	491.39	4.0	−13.3	F	8.20	AF	15–23	4	5.87					0.031	
33R-6, 5	491.78	5.3	−7.2	F	11.30	AF	18–25	4	5.75	6.97	13.60	46.17	5.43	0.033	
33R-6, 45	492.18	2.4	−7.5	F	5.70	TH	480–560	5						0.055	

Notes: * = sample inclination not used in mean colatitude calculation. NRM = natural remanent magnetization intensity. Incl. = inclination of characteristic remanence. PCA type = type of principal component analysis, A = anchored to origin, F = free. MAD = maximum angle of deviation. Demag type = type of demagnetization, AF = alternating field, TH = thermal. Demag steps = demagnetization steps (in mT or °C) used for PCA calculation. N = number of measurements used for PCA calculation. MDF = median destructive field, B_c = coercivity field, B_{cr} = remanent coercivity field. M_s = saturation magnetization, M_r = remanent saturation magnetization. Susceptibility = volume magnetic susceptibility. NS = no stable vector, OV = overprint incompletely removed, MA = MAD > 20°.